






This work was carried out in whole or in part within the framework of the NOMATEN Center of Excellence, supported from the European Union Horizon 2020 research and innovation programme (Grant Agreement No. 857470), the European Regional Development Fund via the Foundation for Polish Science International Research Agenda PLUS programme (Grant No. MAB PLUS/2018/8), *and the initiative of the Ministry of Science and Higher Education 'Support for the activities of Centers of Excellence established in Poland under the Horizon 2020 program' under agreement No. MEiN/2023/DIR/3795.*

This is a copy of the publication which appeared in Phys. Rev. Research 6, 013146, published in February 2024.

DOI: [10.1103/PhysRevResearch.6.013146](https://doi.org/10.1103/PhysRevResearch.6.013146)

Quasilocalized modes in crystalline and partially crystalline high-entropy alloys

Silvia Bonfanti ¹, Roberto Guerra ², Rene Alvarez-Donado,¹ Paweł Sobkowicz,¹ Stefano Zapperi ^{2,3} and Mikko Alava^{1,4}

¹NOMATEN Centre of Excellence, National Center for Nuclear Research, ul. A. Soltana 7, 05-400 Swierk/Otwock, Poland

²Center for Complexity and Biosystems, Department of Physics, University of Milan, via Celoria 16, 20133 Milano, Italy

³CNR - Consiglio Nazionale delle Ricerche, Istituto di Chimica della Materia Condensata e di Tecnologie per l'Energia, Via R. Cozzi 53, 20125 Milano, Italy

⁴Aalto University, Department of Applied Physics, PO Box 11000, 00076 Aalto, Espoo, Finland



(Received 15 March 2023; accepted 5 January 2024; published 6 February 2024)

High entropy alloys (HEAs) are designed by mixing multiple metallic species in nearly the same amount to obtain crystalline or amorphous materials with exceptional mechanical properties. Here we use molecular dynamics simulations to investigate the role of positional and compositional disorder in determining the low-frequency vibrational properties of CrMnFeCoNi HEAs with a varying degree of amorphous order. Our results show that the expected dependence of the density of states on the frequency as $D(\omega) \sim \omega^4$ is recovered for amorphous HEAs and is also observed for partially crystallized alloys with deviations that depend on the degree of crystallization. We find that the quasilocalized vibrations are still visible in crystalline HEAs, albeit suppressed compared to the corresponding amorphous alloys. Our work offers a unified perspective to describe HEA mechanical properties in terms of their vibrational density of states.

DOI: [10.1103/PhysRevResearch.6.013146](https://doi.org/10.1103/PhysRevResearch.6.013146)

I. INTRODUCTION

Metallic alloying has been the key factor in opening up new possibilities for designing materials with desired properties. The discovery of a new class of high entropy alloys (HEAs) represented a breakthrough in the conventional strategy of alloy design: instead of having one or two main atomic species, as in traditional alloys, HEAs consist of several metallic species, five or more, in nearly equal concentration [1]. Mixing many elements results in many possible configurations that can be exploited in the search for those enabling exceptional mechanical properties, e.g., improved hardness and a higher degree of fracture resistance [2,3]. HEAs are mostly studied as crystalline materials, however, the research on their glassy disordered counterpart, namely, HEA glasses, is also attracting a growing interest [4,5]. HEA glasses display high strength and large resistance in high-temperature conditions. In the literature, HEAs often refer only to crystalline configurations [6,7] while their glassy counterparts are denoted high entropy metallic glasses [5]. Here, we use the term HEAs to refer to the ensemble of the possible solid phases, from crystalline to partially crystallized up to amorphous ones. These systems have also become under an experimental focus due to various cocktail effects the mixture of crystalline and amorphous phases brings with it [8–10].

From a structural perspective [see Fig. 1(a)], the distinctive feature of HEA crystals is the presence of compositional

disorder: atomic species are *randomly* distributed across the lattice sites, avoiding repetitive patterns typical of traditional crystals. Amorphous HEAs are instead characterized by positional disorder [11]. The theoretical understanding of the structure-property relation of HEAs is currently missing, hampering the formulation of design principles to get desirable HEAs for target applications.

Here, we shed light on the vibrational properties of HEAs which are essential to rationalize the other physical properties. There is ample evidence that the vibrational density of states $D(\omega)$ of glasses depends on the frequency ω as $D(\omega) \sim \omega^4$ [12–15], exceeding the Debye's contribution typical of three dimensional crystals that depends on ω^2 . The associated low-frequency glassy modes are quasilocalized in space and are found to be related to the mechanical properties [16,17] and the stability of glasses [18]. The law is found to hold independently from the model of glass former, being valid for toy models of glasses with binary interactions [13,19–23] and for more realistic models of silica glasses [24,25]. The quartic law has been shown to be independent of dimensionality [26,27] and temperature, as long as the system remains within its inherent structure [28]. In a recent numerical work [29], the quartic law has also been found to hold in a simple model of a two component Lennard-Jones disordered crystal, where the level of positional disorder has been controlled.

In this work, we investigate the validity of the quartic law for HEAs and explore the role of compositional disorder by simulating the low frequency vibrational properties of the Cantor alloy [7], composed by (Cr,Mn,Fe,Co,Ni) in equiatomic proportion, for different degrees of positional disorder. This is introduced so as to model the presence of local amorphous regions as in experiments [8–10].

Published by the American Physical Society under the terms of the [Creative Commons Attribution 4.0 International license](https://creativecommons.org/licenses/by/4.0/). Further distribution of this work must maintain attribution to the author(s) and the published article's title, journal citation, and DOI.

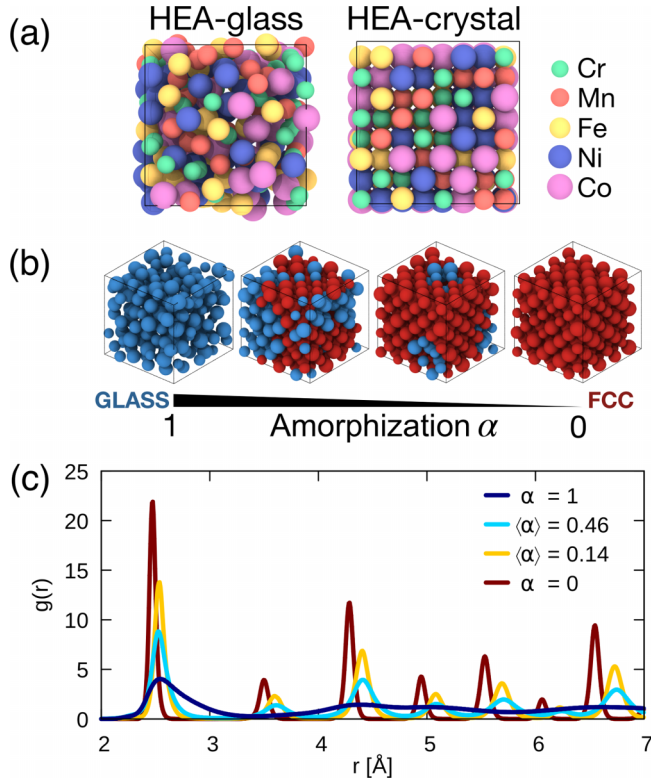


FIG. 1. (a) Concept of HEAs. (Left) HEA glass, characterized by positional disorder. (Right) HEA crystal characterized by positional order and compositional disorder: random distribution of the atom species on the lattice sites. Colors indicate different atomic species. (b) Examples of configurations of Cantor HEAs obtained varying the level of positional disorder α : from glass (left) to intermediates (center) and crystal (right). The red color indicates the FCC structure (FCC), while the blue amorphous state (GLASS). (c) Pair correlation function $g(r)$ for different levels of amorphization.

II. SYSTEM AND PROTOCOL

Simulations are performed in three dimensions with periodic boundary conditions. The interaction between the atoms is given by the modified embedded atom method (MEAM) interatomic potential, implemented in LAMMPS [30]. MEAM is an extension of the class of embedded atom method (EAM) potentials, developed to describe atomic interaction in metallic systems [31]. The potential is constructed to have continuous second derivatives to avoid spurious cutoff effects in the Hessian calculation. For Cantor HEAs, we use the parameters of Ref. [32]. Units are defined based on energy, length, and time in eV, Å, and ps. The choice of the system size to be sufficiently small is made with the aim to disentangle quasilocated modes from phonons as stressed in previous works [23,24].

A. HEA glasses

We generate a set of 9000 samples, each with $N = 200$ atoms randomly placed in the box with a density of $6.65 \times 10^{-24} \text{ g}/\text{Å}^3$ [33]. After an initial 2-ps run with Lennard-Jones interatomic interaction, we switch to the potential for Cantor HEAs and perform subsequent 8 ps of relaxation, and then

equilibrate the system at 2000 K. Finally, we quench to 0 K by structurally relaxing the samples using the fast inertial relaxation engine (FIRE) [34] minimization until the maximum force on each atom is smaller than $10^{-10} \text{ eV}/\text{Å}$.

B. HEA crystals

Since Cantor HEA crystals possess face-centered cubic (FCC) symmetry, we start from a pure FCC lattice of Ni atoms with $N = 256$. Subsequently, we change the atomic species randomly until we obtain equiatomicity, i.e., an equal fraction of atoms for the five elements and use the potential for Cantor HEAs. We then equilibrate the system at 500 K and instantaneously quench to 0 K with FIRE and the above constraint on the forces as stopping criteria. The dataset consists of 920 000 samples.

C. HEA intermediates

To model partially crystallized HEA configurations, we vary the level of positional disorder through a variant of the procedure introduced in Ref. [35]. Starting from one FCC configuration of HEA crystal with $N = 256$ particles, we randomly remove a selected number m of particles and reinsert them in a random position in the box. In our simulations, we choose $m = 1, 5, 10$ and produce, respectively, about 447 000, 256 000, and 41 000 samples for each case. Subsequently, we relax the size of the simulation box to adjust to the new volume and perform again FIRE [34] minimization with the force constraint to relax the system. We further define a parameter $\alpha = 1 - \frac{N_{\text{FCC}}}{N}$, where N_{FCC} is the number of atoms with FCC symmetry, as resulting from adaptive common neighbor analysis calculation [36] using a cutoff radius of 4 Å, which assures the embracement of second neighbors. We checked that all the glass (crystal) structures give $\alpha = 1$ ($\alpha = 0$). The intermediate configurations with a given m produce, after the structural relaxation, a broad range of α values, as shown in the Appendix, Fig. 6. Therefore, we restrict the considered amorphization values by selecting two ranges of α , 0.1–0.3, and 0.4–0.7, corresponding to two sets of samples with average $\langle \alpha \rangle = 0.14$ and $\langle \alpha \rangle = 0.46$, respectively. Details of the distribution of the number of FCC structures for different values of m is reported for completeness in Appendix, Fig. 6.

D. Vibrational modes calculation

The potential energy of the system $U(\mathbf{r}_1, \dots, \mathbf{r}_N)$, with r_i being the i th coordinate of one atom, provides the Hessian matrix \mathbf{H} , which gives, in the harmonic approximation, the frequencies and associated eigenmodes [37]

$$H_{ij}^{\alpha\beta} \equiv \frac{1}{\sqrt{m_i m_j}} \frac{\partial^2 U(\mathbf{r}_1, \dots, \mathbf{r}_N)}{\partial r_i^\alpha \partial r_j^\beta}, \quad (1)$$

where m_i is the mass of the i th atom. By diagonalizing \mathbf{H} , we obtain the modes and eigenvalues in athermal conditions. The frequencies ω_i are obtained from the square root of the eigenvalues.

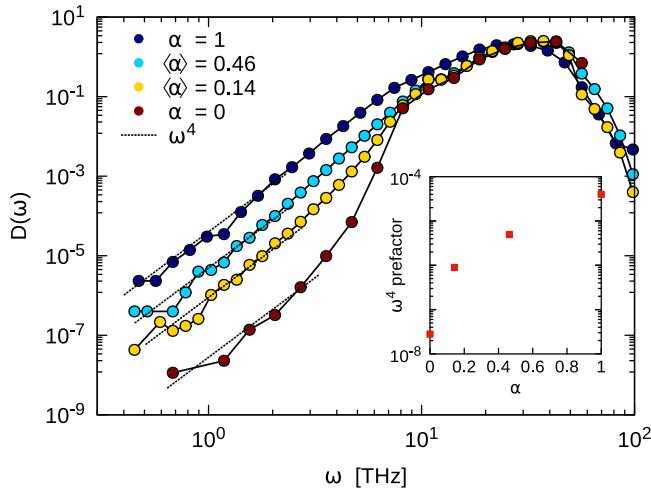


FIG. 2. Vibrational density of states for HEAs with different amorphization degree α ($\alpha = 0$ crystal, $\langle \alpha \rangle = 0.46, 0.14$ intermediates, $\alpha = 1$ glass). The inset shows the fitted values of the prefactor of the density of states versus α .

III. RESULTS

Figure 1(b) reports examples of snapshots of Cantor HEAs for different values of the amorphization parameter α : from left to right, HEA glass with $\alpha = 1$, two HEA intermediates with $\langle \alpha \rangle = 0.46, 0.14$ and HEA crystal with $\alpha = 0$. Note that the different atomic species are marked with different sizes of radius. The color represents the number of FCC structures of the configuration: red atoms possess FCC local positional order while blue atoms disorder. The evolution of the pair correlation function $g(r)$ for different levels of amorphization is reported in Fig. 1(c). Note that the pair correlation function was averaged over 8500 samples. We observe that the shape of the $g(r)$ is consistent with a glass (blue curve) and reaches the typical FCC pattern for the crystal (red curve) as the amorphization is reduced (respectively light blue and yellow curves for $\langle \alpha \rangle = 0.46, 0.14$).

The density of states for different levels of disorder: from glass to crystal, is shown in Fig. 2, which is the main result of this work. Amorphous samples ($\alpha = 1$, blue dots) display the ω^4 law typical of glassy systems, confirming that also HEA glasses show the same universality class as other glassy systems. By decreasing the level of disorder, thus reducing the level of amorphization ($\langle \alpha \rangle = 0.46, 0.14$, light blue and yellow curves respectively), we find that also the partially crystallized configurations show ω^4 trend. However, the magnitude of the density of states also decreases with decreasing α . The suppression is even more evident in the case of HEA-crystals ($\alpha = 0$, red dots), where the ω^4 law is only present at very low frequencies.

The inset of Fig. 2 displays the prefactor of the density of states for HEAs as a function of the amorphization on a log-lin scale, obtained from the fits of the curves with ω^4 at low frequency. The prefactor of HEA crystals interestingly shows a drop that deviates from the amorphous and partially crystallized cases. We checked, however, that choosing slightly different range values for α or changing the number of samples for the average does not significantly affect the

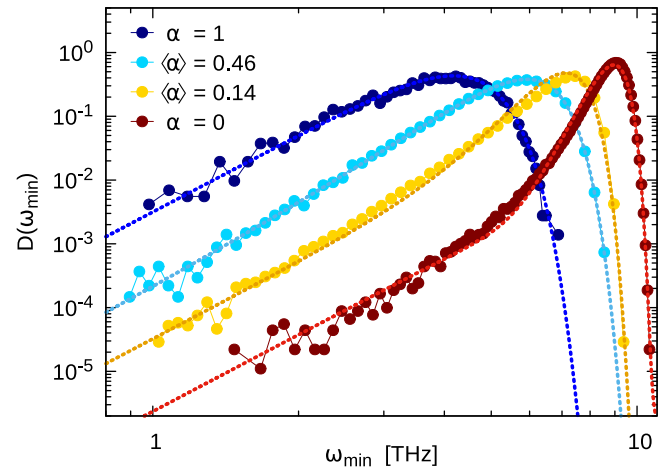


FIG. 3. Distribution of the minimum eigenfrequency ω_{\min} for different amorphization values α . The dotted lines are fit via two Weibull distributions. Fit and data were normalized to unity.

results. Note, also, that the frequency range has been binned in a logarithmic way and changing the binning to linear or the size of the binning does not alter the results. To assess the robustness of the ω^4 law in HEA crystals, we conducted additional Monte Carlo simulations to search for more stable configurations in terms of chemical composition ordering [38]. The results obtained from these HEA crystals show the presence of chemical short-range ordering, and confirm the ω^4 trend of the density of states with a larger prefactor compared to the ideal random case (see the Appendix).

To further examine the scaling range of the ω^4 law, we consider the average of the minimal frequency ω_{\min} for each configuration over the ensemble of configurations is indicated as $\langle \omega_{\min} \rangle$. Extreme value theory implies that the distribution of ω_{\min} should follow the Weibull distribution [39]

$$W(k; \omega_{\min}) = \frac{(k+1)(\Gamma(a))^{k+1}}{\langle \omega_{\min} \rangle^{k+1}} \omega_{\min}^k e^{-\left(\frac{\omega_{\min} \Gamma(a)}{\langle \omega_{\min} \rangle}\right)^{k+1}}, \quad (2)$$

where $\Gamma(x)$ is the Gamma function, and $a = 1 + 1/(k+1)$. For amorphous materials, the parameter k should assume the well-defined value of $k = 4$, in agreement with the power-4 scaling law holding therein. Instead, in the limit of an ideal crystal, one would obtain a unique ω_{\min} value, with $W(\omega_{\min})$ approaching the δ function (i.e., $k \rightarrow \infty$). In our case of partially crystallized HEAs, we, therefore, expect that a combination of (at least) two W distributions is required to account for the multiple failure rates associated with the different constituent phases, with one exhibiting the $k = 4$.

This prediction is tested in Fig. 3, where the fitting of the data is performed by two Weibull functions, one with fixed $k = 4$ and another with free k parameter (see the Appendix Fig. 7 for a detailed plot of the fitting functions). We note that, for decreasing disorder ($\alpha \rightarrow 0$), the peak of the distribution shifts toward higher frequencies, consistently with the appearance of delocalized high-energy modes. By calculating the participation ratio P [40] of the eigenvectors associated to the ω_{\min} for different α we obtained an average $\langle P \rangle = 0.05, 0.13, 0.18, 0.37$ for $\alpha = 1, 0.46, 0.14, 0$, respectively. The distributions $D(P)$ (see Appendix Fig. 8)

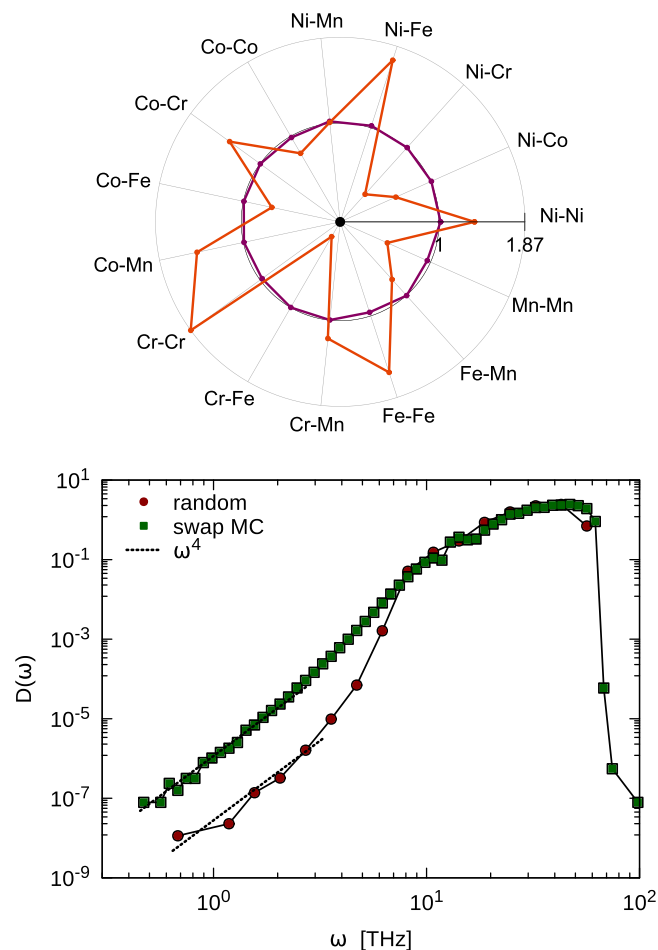


FIG. 4. Top: Warren-Cowley parameters for random solid solutions (red) and configurations obtained with swap MC (green). Clear CSRO is seen. Bottom: Density of states for HEA crystals with random positioning of the atoms in the FCC lattice (circles) or after MC + MD optimization (squares). The evident increase of the $D(\omega)$ amplitude in the optimized samples is associated with local chemical ordering.

are peaked at around $P_l \sim 0.05$ (strong localized modes) for larger amorphous fraction, while a second peak at $P_d \sim 0.45$ (weak localized modes) starts to appear when approaching the crystalline phase, becoming dominant only at $\alpha = 0$. Remarkably, while the $D(P)$ associated with $\alpha = 1$ shows no trace of contributions from P_d , the one associated with $\alpha = 0$, it clearly shows some contribution from P_l which we address to the residual atomic positional perturbation induced by the compositional disorder.

We next show that real materials with chemical short-range ordering (CSRO) plot (see also the Appendix for the method) are, in fact, more affected by the QLM. We plot the average Warren-Cowley parameter, Fig. 4(top), demonstrating that there is CSRO in the Cantor alloy after the hybrid MC + MD procedure, represented by the green dotted curve. We also include the random case, depicted by the red dotted curve, which shows that no specific atomic pairs exhibit a preference to form (circular shape).

Then, on the bottom of Fig. 4 we report the resulting density of states for optimized samples (green squares) in

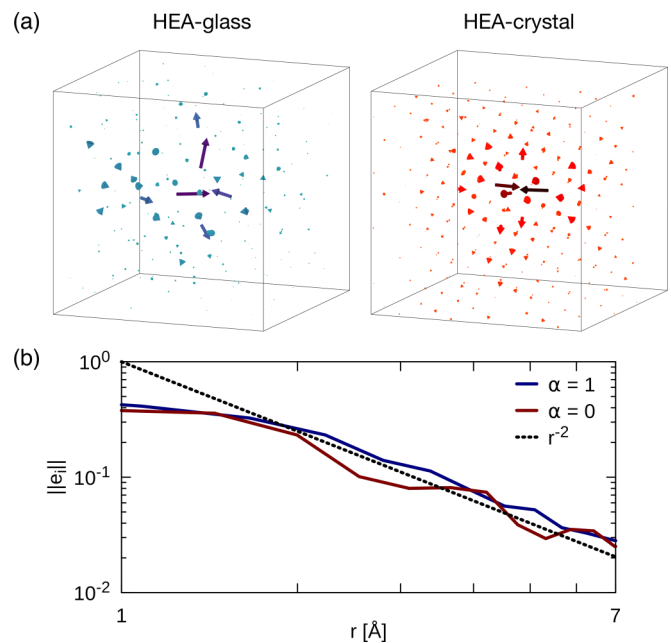


FIG. 5. (a) Orthogonal view of the eigenvectors \hat{e} corresponding to the ω_{\min} for typical configurations of HEA glass (left) and HEA crystal (right). Arrows size has been increased by a factor of 4. The color of the arrows represents the modulus of the vectors: from dark blue ($e = 0.5$) to light blue $e = 0$ for HEA glasses and from dark red ($e = 0.5$) to light red $e = 0$ for HEA crystals. (b) Spatial decay of the quasilocalized modes for HEA glasses and HEA crystals averaged over ten configurations.

comparison with the random ones (red circles). We first note that the ω^4 law is confirmed also in the presence of CSRO, and therefore we expect that it should hold for any HEAs with CSRO. Moreover, we observe that the presence of local compositional ordering leads to a larger prefactor of ω^4 . We expect that the same would occur for systems with $\alpha > 0$ upon swap MC optimization and the resulting short-range order.

Examples of quasilocalized modes for amorphous and crystalline HEAs are shown in Fig. 5(a) (left and right panels, respectively). The arrows indicate the eigenvectors corresponding to the smallest frequency ω_{\min} . Specifically, $\omega_{\min} = 0.9974$ THz and the participation ratio $P = 0.0415$ for the glass, and $\omega_{\min} = 1.4912$ THz and $P = 0.0522$ for the crystal system. Arrows are colored according to the magnitude of the modulus of the vectors.

After visualizing the quasilocalized modes \hat{e} in real space, we focus on the analysis of their spatial decay for both HEA glasses and crystals. We calculate the core of the event by computing the weighted average of the position of the modes with their magnitude, considering only the six particles with the highest $\|\hat{e}_i\|^2$. The spatial decay is defined as the distance r_i of each particle from the core. We consider the average over ten different configurations and bin the value of the distance. Quasilocalized modes are expected to follow r^{-2} at the far field [23], and our results confirm the same trend for both the HEA glasses and HEA crystals, see Fig. 5(b).

Finally, we also computed the participation ratio of all the modes and found that quasilocalized low-frequency modes are characterized by a low participation ratio. This result agrees

with previous investigation on glassy systems [23] (see also Appendix Fig. 8).

IV. SUMMARY AND CONCLUSION

The goal of this work is to examine the low-frequency vibrational properties of HEAs for different levels of amorphization and study to what extent the ω^4 law remains valid. Our results show that the density of states at low-frequency follows the ω^4 nonphononic trend associated with quasilocalized modes in space for all levels of positional disorder. We find that compositional disorder is the leading cause of the presence of quasilocalized modes and observe the ω^4 law also in crystalline HEAs. This is an addition to the density of states of conventional crystals that follows the ω^2 trend in three dimensions. HEA crystals can, therefore, be regarded as intermediate between completely disordered solids (specifically metallic glasses) and ordered solids (pure crystalline metals). Experimentally, glassy-like behaviors were reported in other types of disordered crystals characterized by a small amount of disorder at low temperatures, e.g., Ref. [41]. Literature on HEA crystals at low temperatures is not extensive [42,43], but there might be a possibility that those glassy anomalies are present, considering the presence of quasilocalized modes found in our study.

The compositional disorder in HEA crystals implies that atoms are slightly displaced from the ideal lattice sites causing lattice distortions [44,45] as also revealed experimentally from single-crystal synchrotron x-ray diffraction for the equiatomic Cantor HEA crystals [46]. The measured value for the squared atomic displacement parameter from the ideal FCC sites of a pure metal and at low temperature is $23.5 \pm 0.4 \text{ pm}^2$ [46]. Quasilocalized modes, however, are revealed to be a tool to measure the local disorder being able to capture even the tiny lattice distortions present in HEA crystals. The number of localized modes decreases with increasing order and decreases with chemical ordering. It is an interesting question also how the CSRO impact locally on QLMs and lattice distortion correlates [47]. A separate discussion is necessary for the relation between the vibrational properties of HEA crystals and lattice distortion, which is a task for future research.

ACKNOWLEDGMENTS

We gratefully thank Professor Itamar Procaccia for fruitful discussions. S.B., R.A.-D., P.S., and M.A. are supported by the European Union Horizon 2020 research and innovation program under Grant Agreement No. 857470 and from the European Regional Development Fund via the Foundation for Polish Science International Research Agenda PLUS program Grant No. MAB PLUS/2018/8.

APPENDIX

Figure 6 reports the distribution $D(\alpha)$ of the number of FCC structures in the samples generated by varying the value of $m = 1, 5, 10$ particles. Figure 7 shows the two Weibull functions (continuous and dotted lines of the same color) for each value of amorphization α , used to fit the data in Fig. 3.

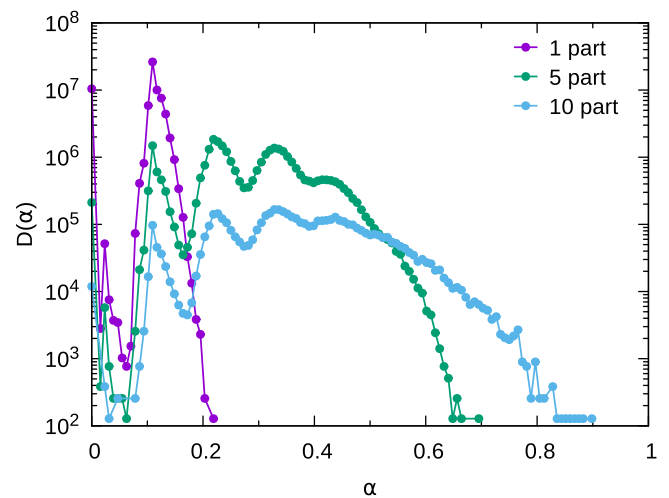


FIG. 6. Distribution of the amorphization degree α for the structures obtained by randomly displacing $m = 1, 5$, or 10 particles starting from an FCC HEA crystal.

For the case of glass where $\alpha = 1$, the two Weibull functions are degenerate. The distributions of the participation ratio $D(P)$ for each different value of α are reported in Fig. 8.

Role of compositional disorder in HEA crystals

HEA crystals are generally assumed to form a random solid solution (RSS) implying that the multiple elements are mixed randomly on the crystal lattice sites. However, emerging evidence suggests that the RSS picture is possible at very high temperatures while, with annealing, a local chemical ordering, also known as chemical short range ordering (CSRO), is formed [38,48–52]. In contrast to RSS, local chemical ordering implies that each atomic species shows a preference for its nearest neighbors: there is a tendency for specific types of atomic pairs to form more often. These local nonrandom arrangements could significantly influence the properties of

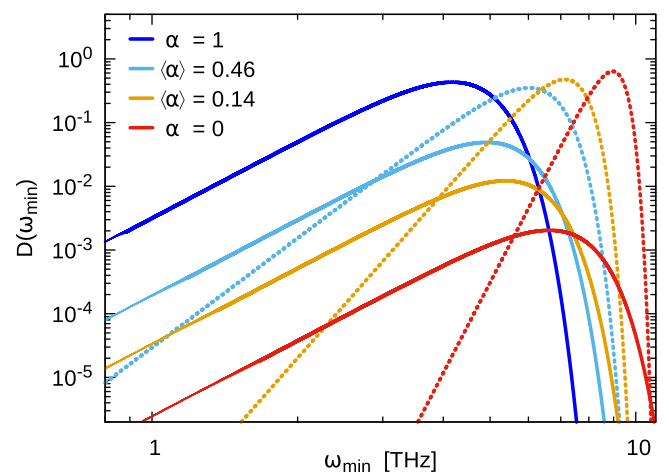


FIG. 7. For each set with amorphization degree α are reported the two Weibull functions whose sum gives the fit of Fig. 3. In the case of pure glass ($\alpha = 1$) the two Weibull functions result degenerate.

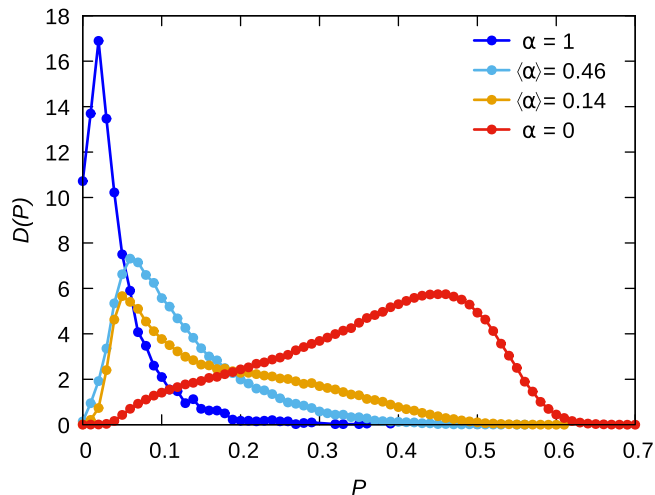


FIG. 8. Distribution of the participation ratio for each set of samples with different amorphization degree α .

HEAs, such as, e.g., dislocation pathways [56] or mechanical properties [52]. The chemical short-range ordering presents challenges in experimental observations, however, it can be observed using numerical techniques such as hybrid Monte Carlo (MC) + molecular dynamics (MD) simulations.

To assess the robustness of ω^4 law in HEA crystals, we further perform MC simulations to search for more stable

configurations in terms of chemical composition ordering. Specifically, following previous approaches, we implement a hybrid swap MC + MD procedure [53–56] as follows. We start from a set of equiatomic samples with atoms placed randomly on the FCC lattice sites. Each sample is initially thermalized at 300 K for 30 ps using a Nose-Hoover thermostat. Then, a sequence of MC + MD steps is performed iteratively. In each MC part, 64 atom pair swaps of different species are attempted. The swaps are accepted or rejected according to the METROPOLIS criterion. After the MC part, 20 MD steps (0.02 ps) at 300 K are carried out to ensure equilibration. Such a sequence is repeated until a stationary state is achieved. Then we extract the configuration and we subsequently perform a positional energy minimization at 0 K and compute the Hessian matrix and the corresponding density of states. We check that all the so-obtained configurations are still FCC and their amorphization parameter α is zero. In total we collect about 400 k optimized configurations that we use for statistics. To quantify the local chemical order in the optimized samples we employ a modified Warren-Cowley parameter [48,53]

$$\Delta\delta_{ij} = N_{ij}/N_{0,ij}, \quad (\text{A1})$$

where N_{ij} is the number of nearest-neighbors pair of atomic species i - j , and $N_{0,ij}$ is the same number in an ideally random solution. Since Cantor HEA corresponds to $M = 5$ components, the possible number of chemical i - j pairs is $M(M + 1)/2 = 15$.

- [1] E. P. George, D. Raabe, and R. O. Ritchie, High-entropy alloys, *Nat. Rev. Mater.* **4**, 515 (2019).
- [2] D. Liu, Q. Yu, S. Kabra, M. Jiang, P. Forna-Kreutzer, R. Zhang, M. Payne, F. Walsh, B. Gludovatz, M. Asta *et al.*, Exceptional fracture toughness of CrCoNi-based medium-and high-entropy alloys at 20 kelvin, *Science* **378**, 978 (2022).
- [3] F. Otto, A. Dlouhy, C. Somsen, H. Bei, G. Eggeler, and E. P. George, The influences of temperature and microstructure on the tensile properties of a CoCrFeMnNi high-entropy alloy, *Acta Mater.* **61**, 5743 (2013).
- [4] W. H. Wang, High-entropy metallic glasses, *JOM* **66**, 2067 (2014).
- [5] Y. Chen, Z.-W. Dai, and J.-Z. Jiang, High entropy metallic glasses: Glass formation, crystallization and properties, *J. Alloys Compd.* **866**, 158852 (2021).
- [6] J.-W. Yeh, S.-K. Chen, S.-J. Lin, J.-Y. Gan, T.-S. Chin, T.-T. Shun, C.-H. Tsau, and S.-Y. Chang, Nanostructured high-entropy alloys with multiple principal elements: novel alloy design concepts and outcomes, *Adv. Eng. Mater.* **6**, 299 (2004).
- [7] B. Cantor, I. T. H. Chang, P. Knight, and A. J. B. Vincent, Microstructural development in equiatomic multicomponent alloys, *Mater. Sci. Eng. A* **375-377**, 213 (2004).
- [8] G. Wu *et al.*, Crystal-glass high-entropy nanocomposites with near theoretical compressive strength and large deformability, *Adv. Mater.* **32**, 2002619 (2020).
- [9] L. L. Xiao *et al.*, Ultra-strong nanostructured CrMnFeCoNi high entropy alloys, *Mater. Design* **194**, 108895 (2020).
- [10] G. Wu *et al.*, Ductility of an ultrastrong glass-crystal nano-dual-phase alloy in sub-micron, *Scr. Mater.* **183**, 17 (2020).
- [11] K. Binder and W. Kob, *Glassy Materials and Disordered Solids: An Introduction to Their Statistical Mechanics* (World Scientific, Singapore, 2011).
- [12] E. Lerner, G. Düring, and E. Bouchbinder, Statistics and properties of low-frequency vibrational modes in structural glasses, *Phys. Rev. Lett.* **117**, 035501 (2016).
- [13] H. Mizuno, H. Shiba, and A. Ikeda, Continuum limit of the vibrational properties of amorphous solids, *Proc. Natl. Acad. Sci. USA* **114**, E9767 (2017).
- [14] M. Shimada, H. Mizuno, M. Wyart, and A. Ikeda, Spatial structure of quasilocalized vibrations in nearly jammed amorphous solids, *Phys. Rev. E* **98**, 060901(R) (2018).
- [15] L. Wang, A. Ninarello, P. Guan, L. Berthier, G. Szamel, and E. Flenner, Low-frequency vibrational modes of stable glasses, *Nat. Commun.* **10**, 26 (2019).
- [16] D. Richard, M. Ozawa, S. Patinet, E. Stanifer, B. Shang, S. A. Ridout, B. Xu, G. Zhang, P. K. Morse, J.-L. Barrat *et al.*, Predicting plasticity in disordered solids from structural indicators, *Phys. Rev. Mater.* **4**, 113609 (2020).
- [17] D. Richard, G. Kapteijns, J. A. Giannini, M. L. Manning, and E. Lerner, Simple and broadly applicable definition of shear transformation zones, *Phys. Rev. Lett.* **126**, 015501 (2021).
- [18] C. Rainone, E. Bouchbinder, and E. Lerner, Pinching a glass reveals key properties of its soft spots, *Proc. Natl. Acad. Sci. USA* **117**, 5228 (2020).

- [19] M. Baity-Jesi, V. Martin-Mayor, G. Parisi, and S. Perez-Gaviro, Soft modes, localization, and two-level systems in spin glasses, *Phys. Rev. Lett.* **115**, 267205 (2015).
- [20] L. Angelani, M. Paoluzzi, G. Parisi, and G. Ruocco, Probing the non-Debye low-frequency excitations in glasses through random pinning, *Proc. Natl. Acad. Sci. USA* **115**, 8700 (2018).
- [21] G. Kapteijns, E. Bouchbinder, and E. Lerner, Universal non-phononic density of states in 2d, 3d, and 4d glasses, *Phys. Rev. Lett.* **121**, 055501 (2018).
- [22] A. Moriel, G. Kapteijns, C. Rainone, J. Zylberg, E. Lerner, and E. Bouchbinder, Wave attenuation in glasses: Rayleigh and generalized-rayleigh scattering scaling, *J. Chem. Phys.* **151**, 104503 (2019).
- [23] E. Lerner and E. Bouchbinder, Low-energy quasilocalized excitations in structural glasses, *J. Chem. Phys.* **155**, 200901 (2021).
- [24] S. Bonfanti, R. Guerra, C. Mondal, I. Procaccia, and S. Zapperi, Universal low-frequency vibrational modes in silica glasses, *Phys. Rev. Lett.* **125**, 085501 (2020).
- [25] D. Richard, K. González-López, G. Kapteijns, R. Pater, T. Vaknin, E. Bouchbinder, and E. Lerner, Universality of the nonphononic vibrational spectrum across different classes of computer glasses, *Phys. Rev. Lett.* **125**, 085502 (2020).
- [26] L. Wang, G. Szamel, and E. Flenner, Low-frequency excess vibrational modes in two-dimensional glasses, *Phys. Rev. Lett.* **127**, 248001 (2021).
- [27] L. Wang, G. Szamel, and E. Flenner, Scaling of the non-phononic spectrum of two-dimensional glasses, *J. Chem. Phys.* **158**, 126101 (2023).
- [28] R. Guerra, S. Bonfanti, I. Procaccia, and S. Zapperi, Universal density of low-frequency states in silica glass at finite temperatures, *Phys. Rev. E* **105**, 054104 (2022).
- [29] E. Lerner and E. Bouchbinder, Disordered crystals reveal soft quasilocalized glassy excitations, *Phys. Rev. Lett.* **129**, 095501 (2022).
- [30] A. P. Thompson, H. M. Aktulga, R. Berger, D. S. Bolintineanu, W. M. Brown, P. S. Crozier, P. J. in 't Veld, A. Kohlmeyer, S. G. Moore, T. D. Nguyen *et al.*, LAMMPS - a flexible simulation tool for particle-based materials modeling at the atomic, meso, and continuum scales, *Comput. Phys. Commun.* **271**, 108171 (2022).
- [31] M. S. Daw and M. I. Baskes, Embedded-atom method: Derivation and application to impurities, surfaces, and other defects in metals, *Phys. Rev. B* **29**, 6443 (1984).
- [32] W.-M. Choi, Y. H. Jo, S. S. Sohn, S. Lee, and B.-J. Lee, Understanding the physical metallurgy of the CoCrFeMnNi high-entropy alloy: an atomistic simulation study, *npj Comput. Mater.* **4**, 1 (2018).
- [33] K. Karimi, A. Esfandiarpour, R. Alvarez-Donado, M. Alava, and S. Papanikolaou, Shear banding instability in multicomponent metallic glasses: Interplay of composition and short-range order, *Phys. Rev. B* **105**, 094117 (2022).
- [34] E. Bitzek, P. Koskinen, F. Gähler, M. Moseler, and P. Gumbsch, Structural relaxation made simple, *Phys. Rev. Lett.* **97**, 170201 (2006).
- [35] C. P. Goodrich, A. J. Liu, and S. R. Nagel, Solids between the mechanical extremes of order and disorder, *Nat. Phys.* **10**, 578 (2014).
- [36] A. Stukowski, Structure identification methods for atomistic simulations of crystalline materials, *Modell. Simul. Mater. Sci. Eng.* **20**, 045021 (2012).
- [37] C. E. Maloney and A. Lemaître, Amorphous systems in athermal, quasistatic shear, *Phys. Rev. E* **74**, 016118 (2006).
- [38] X. Wu, Chemical short-range orders in high-/medium-entropy alloys, *J. Mater. Sci. Technol.* **147**, 189 (2023).
- [39] S. Karmakar, E. Lerner, and I. Procaccia, Statistical physics of the yielding transition in amorphous solids, *Phys. Rev. E* **82**, 055103(R) (2010).
- [40] S. Bonfanti, R. Guerra, C. Mondal, I. Procaccia, and S. Zapperi, Elementary plastic events in amorphous silica, *Phys. Rev. E* **100**, 060602(R) (2019).
- [41] M. Moratalla, J. F. Gebbia, M. A. Ramos, L. C. Pardo, S. Mukhopadhyay, S. Rudić, F. Fernandez-Alonso, F. J. Bermejo, and J. L. Tamarit, Emergence of glassy features in halomethane crystals, *Phys. Rev. B* **99**, 024301 (2019).
- [42] J. Wang, J. Li, Q. Wang, J. Wang, Z. Wang, and C. T. Liu, The incredible excess entropy in high entropy alloys, *Scr. Mater.* **168**, 19 (2019).
- [43] M. Naeem, H. He, S. Harjo, T. Kawasaki, W. Lin, J.-J. Kai, Z. Wu, S. Lan, and X.-L. Wang, Temperature-dependent hardening contributions in CrFeCoNi high-entropy alloy, *Acta Mater.* **221**, 117371 (2021).
- [44] Y. Zhang, T. T. Zuo, Z. Tang, M. C. Gao, K. A. Dahmen, P. K. Liaw, and Z. P. Lu, Microstructures and properties of high-entropy alloys, *Prog. Mater. Sci.* **61**, 1 (2014).
- [45] Q. He and Y. Yang, On lattice distortion in high entropy alloys, *Front. Mater.* **5**, 42 (2018).
- [46] N. L. Okamoto, K. Yuge, K. Tanaka, H. Inui, and E. P. George, Atomic displacement in the CrMnFeCoNi high-entropy alloy—A scaling factor to predict solid solution strengthening, *AIP Adv.* **6**, 125008 (2016).
- [47] K. Sheriff, Y. Cao, T. Smidt, and R. Freitas, Quantifying chemical short-range order in metallic alloys, [arXiv:2311.01545](https://arxiv.org/abs/2311.01545).
- [48] Q. Ding, Y. Zhang, X. Chen, X. Fu, D. Chen, S. Chen, L. Gu, F. Wei, H. Bei, Y. Gao *et al.*, Tuning element distribution, structure and properties by composition in high-entropy alloys, *Nature (London)* **574**, 223 (2019).
- [49] F. D. C. Garcia Filho, R. O. Ritchie, M. A. Meyers, and S. N. Monteiro, Cantor-derived medium-entropy alloys: bridging the gap between traditional metallic and high-entropy alloys, *J. Mater. Res. Technol.* **17**, 1868 (2022).
- [50] X. Chen, Q. Wang, Z. Cheng, M. Zhu, H. Zhou, P. Jiang, L. Zhou, Q. Xue, F. Yuan, J. Zhu *et al.*, Direct observation of chemical short-range order in a medium-entropy alloy, *Nature (London)* **592**, 712 (2021).
- [51] Q. F. He, P. H. Tang, H. A. Chen, S. Lan, J. G. Wang, J. H. Luan, M. Du, Y. Liu, C. T. Liu, C. W. Pao *et al.*, Understanding chemical short-range ordering/demixing coupled with lattice distortion in solid solution high entropy alloys, *Acta Mater.* **216**, 117140 (2021).
- [52] S. Chen, Z. H. Aitken, S. Pattamatta, Z. Wu, Z. G. Yu, D. J. Srolovitz, P. K. Liaw, and Y. W. Zhang, Simultaneously enhancing the ultimate strength and ductility of high-entropy alloys via short-range ordering, *Nat. Commun.* **12**, 4953 (2021).
- [53] I. Lobzenko, D. Wei, M. Itakura, Y. Shiihara, and T. Tsuru, Improved mechanical properties of Co-free high-entropy Can-

- tor alloy: A first-principles study, [Results Mater.](#) **17**, 100364 (2023).
- [54] J. Ding, Q. Yu, M. Asta, and R. O. Ritchie, Tunable stacking fault energies by tailoring local chemical order in CrCoNi medium-entropy alloys, [Proc. Natl. Acad. Sci. USA](#) **115**, 8919 (2018).
- [55] M. Widom, W. P. Huhn, S. Maiti, and W. Steurer, Hybrid Monte Carlo/molecular dynamics simulation of a refractory metal high entropy alloy, [Metall. Mater. Trans. A](#) **45**, 196 (2014).
- [56] Q.-J. Li, H. Sheng, and E. Ma, Strengthening in multi-principal element alloys with local-chemical-order roughened dislocation pathways, [Nat. Commun.](#) **10**, 3563 (2019).